BIOCHEMISTRY
including biophysical chemistry & molecular biology
Article

Biochemistry **2010,** *49,* 3703–3714 3703
DOI: 10.1021/bi1000036

Heterogeneity and Dynamics of the Ligand Recognition Mode in Purine-Sensing Riboswitches†

Niyati Jain,‡ Liang Zhao,‡ John D. Liu,§ and Tianbing Xia*

Department of Molecular and Cell Biology, The University of Texas at Dallas, Richardson, Texas 75080-3021. ‡*These authors contributed equally to this work.* §*Current address: Department of Biochemistry and Cell Biology, Rice University, Houston, TX 77251-1892.*

Received January 1, 2010; Revised Manuscript Received March 24, 2010

ABSTRACT: High-resolution crystal structures and biophysical analyses of purine-sensing riboswitches have revealed that a network of hydrogen bonding interactions appear to be largey responsible for discrimination of cognate ligands against structurally related compounds. Here we report that by using femtosecond time-resolved fluorescence spectroscopy to capture the ultrafast decay dynamics of the 2-aminopurine base as the ligand, we have detected the presence of multiple conformations of the ligand within the binding pockets of one guanine-sensing and two adenine-sensing riboswitches. All three riboswitches have similar conformational distributions of the ligand-bound state. The known crystal structures represent the global minimum that accounts for 50−60% of the population, where there is no significant stacking interaction between the ligand and bases of the binding pocket, but the hydrogen-bonding cage collectively provides an electronic environment that promotes an ultrafast (∼1 ps) charge transfer pathway. The ligand also samples multiple conformations in which it significantly stacks with either the adenine or the uracil bases of the A21-U75 and A52-U22 base pairs that form the ceiling and floor of the binding pocket, respectively, but favors the larger adenine bases. These alternative conformations with well-defined base stacking interactions are ∼1−1.5 kcal/mol higher in ΔG° than the global minimum and have distinct charge transfer dynamics within the picosecond to nanosecond time regime. Inside the pocket, the purine ligand undergoes dynamic motion on the low nanosecond time scale, sampling the multiple conformations based on time-resolved anisotropy decay dynamics. These results allowed a description of the energy landscape of the bound ligand with intricate details and demonstrated the elastic nature of the ligand recognition mode by the purine-sensing riboswitches, where there is a dynamic balance between hydrogen bonding and base stacking interactions, yielding the high affinity and specificity by the aptamer domain.

RNAs are dynamic molecules, and they interconvert between different conformational states over broad ranges of time scales and length scales (*1*), reflecting their structural elasticity and plasticity. The resulting conformational complexity needs to be characterized by a very rugged energy landscape (*2*, *3*), and conformational dynamics play a significant role in enhancing their functional capacity (*4*). Therefore, it is important to characterize the shape of the whole energy landscape and its full range of dynamics, including those on ultrafast time scales to slow time scales. These characterizations require quantitative resolution of an ensemble of heterogeneous conformations into individual subpopulations, which is still challenging.

Riboswitch RNAs are widespread metabolite-sensing *cis*-regulatory elements (*5*), typically located in the 5′-untranslated region of mRNA adjacent to ∼2% bacterial genes involved in the synthesis, transport, or salvage of essential metabolites (*6*). Currently, there are more than a dozen classes of riboswitches that have been identified that recognize diverse compounds. Riboswitches have quickly become a new paradigm for understanding the principles of RNA folding and dynamics, ligand recognition, and regulatory functions (*5*, *7*), opening up exciting new research opportunities in genetics, structural biology, and ultimately therapeutics (*8*). Riboswitches are generally composed of two modular domains: an aptamer domain that folds into a well-structured receptor for the metabolites serving as a precision sensor for bacteria to monitor the intracellular concentration of various metabolites and an expression platform located immediately downstream from the aptamer domain. By switching between two mutually exclusive alternative structures in response to specific metabolite ligands, the two domains function together to transduce the chemical signals into altered patterns of gene expression at either transcriptional or translational levels (*5*).

Purine-sensing riboswitches are among the most studied. So far, there are four known classes of riboswitches that recognize purines or modified purines (*9*). A wide variety of biochemical, genetic, biophysical, structural, and computational approaches have been used to investigate various aspects of these purine riboswitches. One of the common structural features of all four classes is the fact that they use a conserved pyrimidine residue to form a canonical Watson−Crick base pair with the purine ligand to achieve high levels of specificity (*9*). Three of the four classes are closely related and share sequence, secondary, and tertiary folding. For the two subclasses of adenine- and guanine-sensing

†This work was partially supported by the THECB Norman Hackerman Advance Research Program (009741-0004-2006 and 009741-0015-2007) and the Robert A. Welch Foundation (AT-1645).

*To whom correspondence should be addressed. E-mail: tianbing.xia@utdallas.edu. Phone: (972) 883-6328. Fax: (972) 883-2409.

Published on Web 03/29/2010

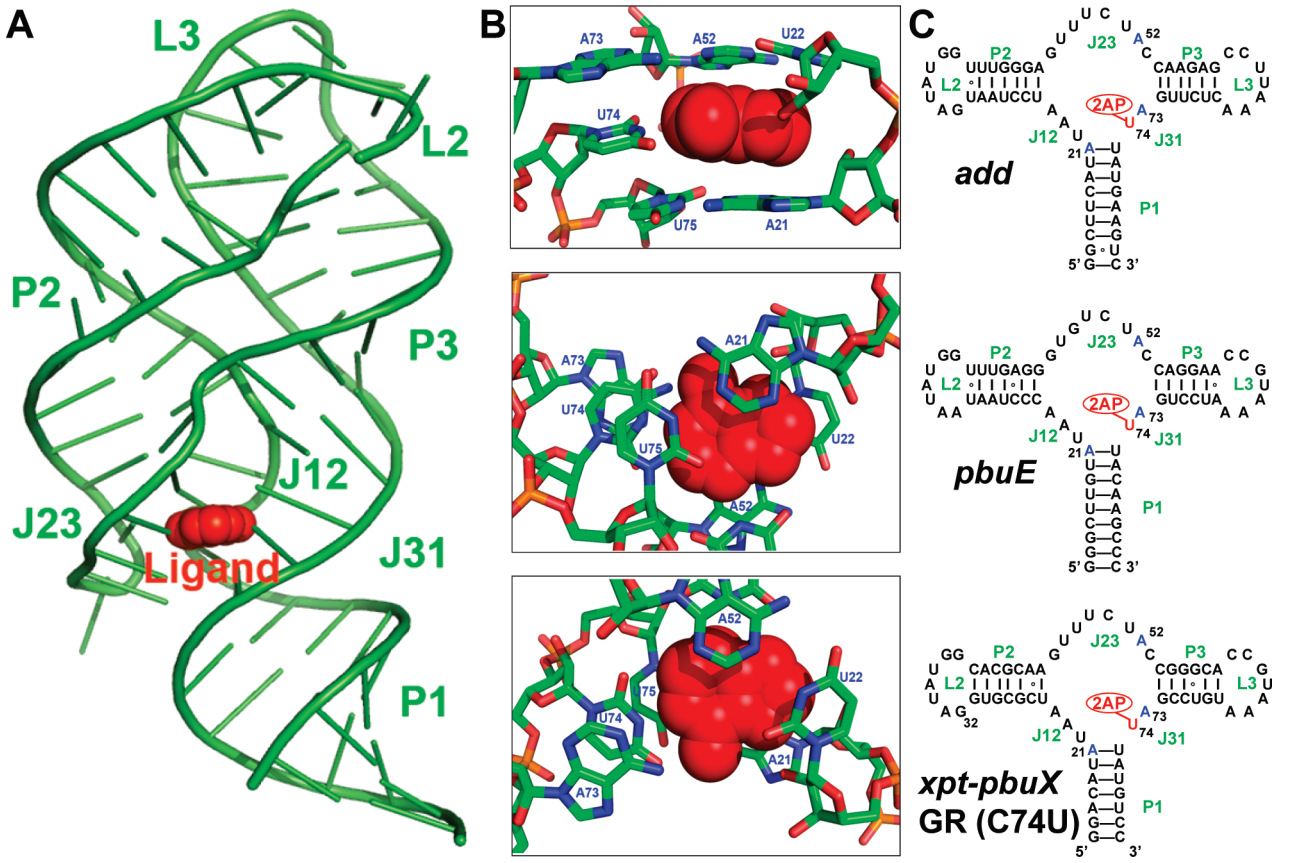

FIGURE 1: Structural models of the aptamer domain of purine-sensing riboswitches. (A) Crystal structure of the aptamer domain of the *add* A-riboswitch (*13*). Helical regions (P1−P3), loops (L2 and L3), and junction regions (J12, J23, and J31) are labeled. The adenine ligand (red) is shown as a space-filling model. (B) Close-up views of part of the binding pocket viewed from the side (top), bottom (middle), or top (bottom) of the *add* riboswitch showing a lack of significant direct base stacking between the ligand and bases forming the ceiling and floor of the pocket (*13*). The ligand is shown as a space-filling model; some surrounding bases forming the pocket that are relevant in this study are labeled, and others have been omitted for the sake of clarity. (C) Secondary structural representations of the wild-type *add* A-riboswitch (top), the *pbuE* A-riboswitch (middle), and the *xpt-pbuX* G-riboswitch with a C74U mutation (bottom), used in this study. Helical regions (P1−P3), loops (L2 and L3), and junction regions (J12, J23, and J31) are labeled, with U74 colored red (base pairing with the 2AP ligand) and A21, A52, and A73 (replaced with 7-deazaadenine in some constructs) colored blue.

riboswitches that recognize the purine bases, the aptamer domains are able to discriminate closely related purine compounds (*10*, *11*). The available X-ray crystal structures (Figure 1A) show that they share nearly identical tertiary folding when bound to cognate ligands, including adenine, guanine, and hypoxanthine (*12*−*14*), or a number of analogues (*15*, *16*). In the ligand-bound state, the aptamer domains fold into a compact structure built from a three-way junction in which the two helices, P2 and P3, are held in parallel through loop−loop tertiary interactions between L2 and L3. The folding creates a binding pocket formed by the highly conserved nucleotides at the three-way junction. The binding pocket is composed of five-tiered base triples that form the ceiling and floor (*12*−*14*). The specificity of recognition is mostly conferred by Watson−Crick base pairing interactions between pyrimidine base Y74 (U for the adenine sensor and C for the guanine sensor) and the purine ligands (Figure 1B). All functional groups of the purine ligands are critical for high-affinity and high-specificity recognition through an intricate network of hydrogen bonding interactions (*10*, *11*, *14*, *15*). It appears, however, that the position of the ligand within the pocket is not optimized for any significant direct stacking interaction with bases of the aptamer (Figure 1B), and hydrogen bonding seems to play a dominant role in ligand-specific recognition (*14*). This has been hypothesized as the origin of the high specificity (*14*) because base stacking interactions are more nonspecific than hydrogen bonding interactions. This is an interesting feature of recognition of such aromatic ligands, as generally the stabilizing energy driving RNA folding largely comes from extensive base−base stacking interactions.

The available high-resolution crystal structures provide a few static images for these riboswitch RNAs in the ligand-bound state that form the basis for understanding the structural complexity required for specific ligand recognition. They may represent, however, only an average or a single frame of an ensemble of conformations, even for the relatively more well-defined bound state. We hypothesize that the observed lack of direct base stacking interaction on ligand recognition by purine riboswitches in the crystal structures only represents one frame of a complex structural ensemble for the ligand-bound state, and more modes of interactions, particularly dynamic stacking interactions between the purine ligand and the bases forming the binding pocket, may coexist dynamically in the solution state. In addition, because the ligand appears to be completely buried in the binding pocket, we wonder if there is any room for dynamic motions of the ligand that may be coupled to the motions of the other regions of the RNA in the complexed state. These two questions may in fact be closely related as such motion would lead to sampling of multiple states, leading to different modes of interactions between the ligand and the pocket in different states. Because of the link between ligand binding by the aptamer

domain and the structural switching in the expression platform, it is crucial to understand the physical and chemical nature of ligand−aptamer recognition to elucidate the functional role of dynamics in the riboregulation mechanism.

To specifically investigate RNA dynamics at different time regimes, appropriate techniques need to be employed (*4*). Currently, it is still difficult to define the precise structural nature of the multiple conformations of RNA, particularly when some conformations are populated at an only minor abundance or transiently. Capturing these alternative conformations helps establish a unified picture of how recognition of a dynamic structure might occur through conformational selection or induced fit (*2*, *3*). Time-resolved spectroscopy with low time resolution may resolve some events of conformational transitions on much slower time scales, but may miss those that occur within the time resolution, and sometimes cannot determine whether the observed complex kinetics arise from static heterogeneity of the structures or dynamic motions on time scales similar to the intrinsic decay of signals.

To extend the range of RNA conformational dynamics that can be studied and resolve the complex ensemble into well-defined subpopulations, we have begun to harness the power of ultrafast time-resolved fluorescence spectroscopy (*17*−*23*). Experimentally, an ultrafast laser pulse excites an incorporated fluorophore to generate coherent excitation among the conformational subpopulations, and a second pulse following a variable delay time monitors the distinct temporal characteristics of the fluorescence decays of each subpopulation. Different RNA conformations within an ensemble may provide different local electronic environments for a site-specifically incorporated probe, causing its fluorescence to decay on distinct time scales characteristic of the structures and specific interactions involved. Therefore, the intrinsic heterogeneous nature of the RNA structures renders the overall fluorescence decay profile multiphasic, where each resolvable decay component potentially reflects the nature of the structural contexts surrounding the probe characteristic of a subpopulation. Resolving the time scales and amplitudes of each decay component within a single decay profile provides useful information that can be meaningfully interpreted in terms of heterogeneous RNA conformations (*21*). The number of such distinct decay components and their relative amplitudes relate to the minimal number of conformational substates and their population distributions (*24*), thus revealing unique structural as well as thermodynamic information that may be at least partly hidden with other techniques.

Recent studies on nanosecond time-resolved probing of 2-aminopurine (2AP)[1] bound to the *pbuE* adenine-sensing and *xpt-pbuX* guanine-sensing riboswitches showed multiple decay components on the nanosecond time scale, suggesting heterogeneity of the ligand-bound state (*25*, *26*). Decay on the picosecond to nanosecond time scale, however, was not adequately resolved; therefore, important information may have been missed. In addition, no comparisons of these fluorescence decay profiles with the *add* adenine-sensing riboswitches have been made. In this report, we demonstrate that by capturing the ultrafast fluorescence quenching dynamics for the 2AP ligand bound in the pockets of all three purine-sensing riboswitches, we can precisely and quantitatively define heterogeneous modes of base stacking interactions between the ligand and the bases of the pockets present in the multiple alternative conformations, allowing a detailed and more complete description of the shape of the energy landscape for the ligand-bound state. The time scale of the base motions inside the pocket can also be monitored by fluorescence anisotropy decay. Such a strategy provides a deeper level of unique structural information beyond that which can be obtained via other techniques.

EXPERIMENTAL PROCEDURES

Materials. 2-Aminopurine (2AP) was purchased from Sigma and used as is without further purification. A stock solution of 10 mM 2AP was used to prepare 2AP−RNA complexes. All riboswitch RNA constructs were synthesized by Dharmacon (Lafayette, CO) and purified by PAGE. RNA concentrations were calculated from the UV absorbance at 260 nm using extinction coefficients provided by Dharmacon. Riboswitch RNAs were annealed in a buffer of 50 mM Na-MOPS, 100 mM NaCl or KCl, and 2 mM $MgCl_2$ (pH 7.5) by being heated to 95 °C for 2 min and allowed to cool slowly, following established protocols (*14*).

Steady State Fluorescence Spectroscopy. Steady state fluorescence emission spectra were recorded at room temperature on a Shimadzu spectrofluorophotometer (RF-5301PC). The 2AP concentration was 10 μM in all samples, and the concentrations of RNAs in the complex samples were 40−50 μM, in a buffer of 50 mM Na-MOPS, 100 mM KCl, and 2 mM $MgCl_2$ (pH 7.5). The excitation wavelength was 320 nm, and emissions were collected from 340 to 500 nm.

Femtosecond Time-Resolved Fluorescence Up-Conversion. The experimental setup and technique for femtosecond time-resolved fluorescence up-conversion have been published previously (*23*, *27*, *28*). Briefly, femtosecond pulses (~120 fs, 800 nm, ~2.3 mJ) are generated from a Ti:sapphire laser system (Spectra Physics). The pulse is split equally to pump two optical parametric amplifiers (OPAs). The signal output from one OPA is quadrupled to generate the excitation pump pulse at 320 nm. The remainder of the fundamental 800 nm is used as the probe pulse. Samples contain 30 μM 2AP and 120−150 μM RNAs in a buffer of 50 mM Na-MOPS, 100 mM NaCl or KCl, and 2 mM $MgCl_2$ (pH 7.5) at 22 °C. The emission from the sample cell is collected by a pair of parabolic focus mirrors and mixed with the fundamental in a BBO crystal. The up-converted signal at 257 nm (up-converted from 380 nm) is detected by a photomultiplier after passing through a double-grating monochromator. For magic angle experiments, the pump beam polarization is set at the magic angle (54.7°) with respect to fluorescence polarization set by the BBO crystal, to avoid complications from orientational motions. In principle, the full femtosecond time-resolved emission spectrum, as opposed to single-wavelength detection mainly used here, also contains rich information, particularly solvation dynamics (*29*, *30*) and DNA dynamics (*31*) on the ultrafast time scale. Although sometimes obtaining the full time-resolved emission spectrum may be desirable, our fluorescence up-conversion experiments were performed by monitoring quenching dynamics of 2AP at a single wavelength around the emission peak (380 nm). Under this condition, the population of this electronic energy state is mostly at steady state with respect to the ultrafast hydration process, and the hydration dynamic does not produce any feature in the transient (neither decay nor rise) on the ultrafast time scale of our interests (*29*); therefore, any ultrafast dynamics observed can be

[1]Abbreviations: 2AP, 2-aminopurine; X, 7-deazaadenine; ITC, isothermal calorimetry; fwhm, full width at half-maximum; OPA, optical parametric amplifier; PAGE, polyacrylamide gel electrophoresis.

attributed to direct charge transfer reactions, and interpretation of the dynamic information is more straightforward.

Data Analysis of Ultrafast Fluorescence Decay Dynamics. The fluorescence decay profile can be represented by a sum of multiple exponential functions convoluted by a Gaussian instrument response function (eq 1) (*23*, *27*):

$$F(t) = \sum_{i=1}^{n} A_i \exp\left(-\frac{t-t_0}{\tau_i}\right) \times \exp\left(\frac{\Delta^2}{4\tau_i^2}\right)\left[1+\mathrm{erf}\left(\frac{t-t_0-\Delta^2/2\tau_i}{\Delta}\right)\right] \quad (1)$$

where τ_i values and A_i values are the decay lifetimes and the preexponential amplitudes, respectively, for the ith decay component, t_0 is time zero, Δ is the width of the instrument response function (cross correlation, typically 500−600 fs determined by recording the Raman emission profile for solvent water), and erf is the error function.

Mathematical software Scientist was used to analyze the ultrafast dynamics data at the magic angle. The number of exponential functions (eq 1) needed to fit a fluorescence decay profile was first determined. Fitting of decay profiles by two, three, and four exponential terms was tested, and the statistical significance of additional terms was analyzed by χ^2 and F tests. Typically, the decay profiles need to be fitted by four exponential terms with well-separated time constants ranging from subpicoseconds to nanoseconds (*22*, *23*). Figure S2 of the Supporting Information shows an example of the residual plots from fitting a decay curve by two-, three-, or four-exponential functions. Apparently, for this decay curve (*pbuE* WT), the four-exponential function fits much better than the two- and three-exponential functions. This is typically the case when there is an ultrafast approximately picosecond component. F values between the three- and four-exponential fits for all decay dynamics are listed in Table S1 of the Supporting Information. All of these values are small, justifying the necessity of using four-exponential functions. The parameter for the slowest component is fixed at the average value (11.3 ns) of the observed lifetimes for free 2AP base, 9-methyl-2AP, and 2AP-riboside (ranging from 10.4 to 11.8 ns) (*32*). This is because the time window of the femtosecond experiments (up to 600 ps) is too short to uniquely determine this slowest decay component. The specific choice of the fixed values for this component on the order of 10−11 ns does not affect the fitting of the faster components, but our testing indicated that the fitting may not converge if it is not fixed (*20*). Components that are typically on the order of hundreds of picoseconds need not be fixed because they can still be sufficiently determined with data collected over the time window. Hundreds of transients were collected to give an average decay profile, with uncertainty in the fitted parameters within 5%.

Femtosecond Time-Resolved Anisotropy. Time-resolved fluorescence anisotropy decay measurements provide useful information about the actual time scale of base dynamic motion of the probe in the context of RNA structures. Time-resolved anisotropy, $r(t)$, is defined in eq 2 (*24*):

$$r(t) = \frac{I_{\parallel}(t) - I_{\perp}(t)}{I_{\parallel}(t) + 2I_{\perp}(t)} \quad (2)$$

where $I_{\parallel}(t)$ and $I_{\perp}(t)$ are calibrated time-dependent fluorescence intensities with emission polarization parallel and perpendicular, respectively, to that of the excitation, collected separately (*20*, *22*, *23*). To account for possible excitation power fluctuation between the two separate independent measurements, the fluorescence intensities for a solution of free 2AP base were measured at two time delay points, one in the negative time regime (e.g., −10 ps) and the other at a long delay time (e.g., 400 ps), following each transient acquisition of the RNA constructs. The fluorescence intensity of 2AP at −10 ps was used for background correction. At a time delay of 400 ps, the anisotropy of free 2AP base should have completely decayed to zero, and an identical intensity of 2AP fluorescence should be observed between parallel and perpendicular polarizations. The differences in the intensities between these two time delays of −10 and 400 ps for parallel polarization and perpendicular polarization were used to calibrate the two polarization transients of RNA constructs. The femtosecond time-resolved anisotropy, $r(t)$, constructed using eq 2, was then fitted with a multiple-exponential function. Often, there is one slow decay term on a long nanosecond time scale that represents the tumbling of the entire molecule. Additional faster decay terms on picosecond to nanosecond time scales represent segmental or internal motions of the probe that reflect its intrinsic mobility (*20*, *22*).

Isothermal Titration Calorimetry (*ITC*). All the ITC titrations of the 2AP base with various RNA constructs were performed on a MicroCal iTC_{200} microcalorimeter (Microcal, Inc.). RNAs (10 μM) were annealed in a buffer of 50 mM Na-MOPS, 100 mM NaCl, and 2 mM $MgCl_2$ (pH 7.5). The 2AP solution (100−150 μM) was prepared in the identical buffer at a concentration 10−15-fold higher than the RNA concentrations (*33*). All the ITC experiments were conducted at 30 °C. A volume of 300 μL of RNA solution was carefully loaded in the cell using the syringe to prevent the formation of air bubbles. The 2AP ligand was titrated into the sample cell containing the RNA. The parameters were set up such that the number of injections ranged from 20 to 25, the stirring speed in the sample cell was 1000 rpm with a starting differential power setup at ~5 μcal/s, and the injection time was 3 min with an initial delay of 1 min. Collected data were fitted to a model with a single set of equivalent binding sites represented by eq 3 (*14*) using Origin 7.0 ITC (Microcal Software Inc.):

$$q = V[\mathrm{RNA}]\Delta H\left(\frac{K_a[\mathrm{L}]_i^n}{1+K_a[\mathrm{L}]_i^n} - \frac{K_a[\mathrm{L}]_{i-1}^n}{1+K_a[\mathrm{L}]_{i-1}^n}\right) \quad (3)$$

where q is the experimentally measured heat released, V is the default volume of the reaction cell (200.15 μL), $[\mathrm{L}]_i$ is the ligand concentration at the ith injection, n is the number of binding sites on the receptor, and K_a is the association constant (inverse of the dissociation constant, K_d).

RESULTS

Multiple Interaction Modes of the Ligand in the Binding Pocket Are Detected. We obtained two adenine-sensing riboswitch RNAs (*add* from *Vibrio vulnificus* and *pbuE* from *Bacillus subtilis*) and a guanine-sensing riboswitch (*xpt-pbuX* from *B. subtilis*) with a C74U mutation that confers specificity to adenine (*14*) (Figure 1C). All three RNAs can bind 2AP as an equivalent ligand (*11*, *14*, *25*, *34*, *35*). The free 2AP base has a natural fluorescence lifetime of 10−11 ns (*32*), and charge transfer reaction due to direct base−base stacking is the main nonradiative decay pathway that causes the large reduction in the fluorescence quantum yield, shortening the lifetime so that it falls

within the picosecond to nanosecond regime depending on the identity of the stacked bases (*27*, *36*). This allows us to probe the physical nature of ligand recognition in the binding pockets of these RNAs by monitoring the ultrafast fluorescence decay profiles for the bound 2AP probe. The steady state fluorescence of 2AP has been previously shown to be quenched upon binding to these riboswitches (*14*, *34*, *35*, *37*), as also confirmed by us (Figure S1 of the Supporting Information), consistent with the presence of quenching dynamics on time scales faster than the ~11 ns natural lifetime of free 2AP (*25*, *26*).

Figure 2 shows the femtosecond time-resolved fluorescence decays of the 2AP probe bound to the three wild-type (WT) riboswitches at 2 mM Mg^{2+}, compared to that of the free 2AP base. As expected, the profile for free 2AP shows a lack of significant decay within the subnanosecond time window because of its intrinsic long lifetime. The decay profiles for the 2AP probe bound to the three riboswitches, however, are similar to each other in overall decay dynamics, but all have very complex profiles. The decays can be best fitted by four lifetimes with various relative amplitudes (Table S1 of the Supporting Information). The observed ~11 ns components (τ_4) with low amplitudes (4−5%) for the three WT complexes apparently represent residual free 2AP base that is not bound to the RNAs, as the total amplitude of this component decreases upon titration of RNAs into the 2AP solution to form the complexes (data not shown). This component is therefore not discussed further because we are interested in only the probe bound to the RNAs. There is no significant decrease in the fluorescence intensity at time zero within our femtosecond time resolution when compared to that of the free 2AP, suggesting there is no significant unresolved quenching dynamics faster than the femtosecond time resolution that contribute to the overall reduction of the quantum yield. In addition, there are no significant quenching dynamics on a time scale longer than 1 ns. This is a nontrivial observation because on the basis of the crystal structures, the ligand in the cavity is practically inaccessible to the solvent (*13*). It is known that a low-polarity environment (apolar solvent) can significantly reduce the quantum yield of 2AP due to the lifetime being shortened from ~11 ns to a few nanoseconds, but no picosecond components have been detected in such a low-polarity environment (*27*). The lack of significant decay components on the approximately nanosecond time scale for bound 2AP suggests that the polarity of the interior of the binding pocket is similar to that of the aqueous or alcohol media, which was found for the interior of the DNA duplex (*38*).

The three observed ultrafast decay components on the picosecond time scale (τ_1 = 0.6−1.1 ps, τ_2 = 5.5−11 ps, and τ_3 = 249−283 ps) of various amplitudes that are robust among the three complexes (Table 1) together contribute to the previously observed significant reduction of the steady state quantum yield of 2AP upon binding to these RNAs (*14*, *25*, *34*, *35*, *37*) (see also Figure S1 of the Supporting Information). In Table 1, the total amplitudes of these three components have been renormalized to unity, excluding that of τ_4. The similarity in the decay dynamics profiles among the three RNAs suggests that there are common origins that lead to the quenching of 2AP excited states in the binding pocket, consistent with their conserved tertiary folding (*12*, *13*). These observed picosecond components for all three complexes indicate that charge transfer has to be the main quenching pathway of 2AP fluorescence when bound to these RNAs. The presence of multiple well-resolved decay dynamics components with distinct time scales indicates that there are

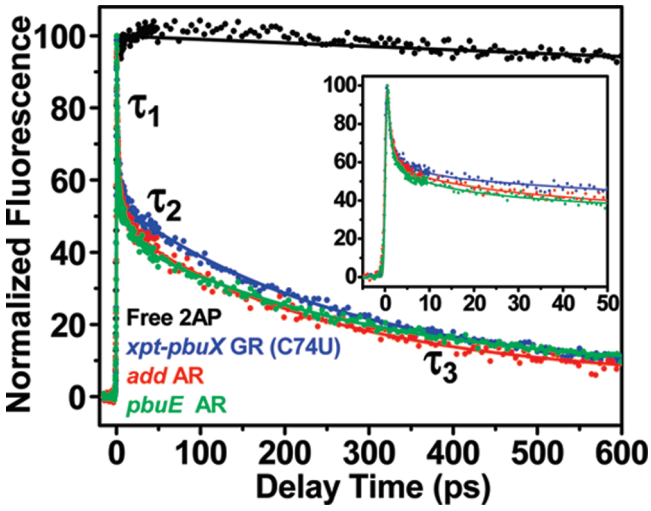

FIGURE 2: Ultrafast time-resolved fluorescence decay dynamics profiles (measured at the magic angle) of free 2AP (black) and 2AP bound to wild-type *xpt-pbuX* GR (C74U) (blue), *add* (red), and *pbuE* (green) riboswitches. Data were collected in a buffer that consisted of 50 mM Na-MOPS, 100 mM NaCl or KCl, and 2 mM Mg^{2+} (pH 7.5) at 22 °C. Concentrations of 2AP and RNAs were 30 and 120−150 μM, respectively. The inset shows a shorter time window to show the ultrafast components.

Table 1: Parameters of Femtosecond Time-Resolved Fluorescence Quenching Dynamics of 2AP Bound to Riboswitches[a]

riboswitch construct[b]	τ_1 (ps)	A_1 (%)	τ_2 (ps)	A_2 (%)	τ_3 (ps)	A_3 (%)
xpt-pbuX-GR (C74U)-WT	0.6	55	5.5	11	269	34
xpt-pbuX-GR (C74U)-A21X	1.2	56	13	29	91	15
xpt-pbuX-GR (C74U)-A52X	1.3	46	13	46	199	8
xpt-pbuX-GR (C74U)-A73X	0.9	58	10	12	226	30
pbuE-WT	0.8	61	11	11	283	28
pbuE-A21X	1.5	53	18	34	117	13
pbuE-A52X	1.4	57	16	35	287	8
pbuE-A73X	0.9	50	8	18	208	32
add-WT	1.1	51	11	11	249	38
add-A21X	2.0	36	23	54	200	10
add-A52X	2.5	35	15	54	190	11
add-A21X/A52X	0.6	63	6.2	33	85	4
add-A73X	0.5	56	5	14	200	30

[a]Decay lifetimes and amplitudes are represented by τ and A, respectively. Only the parameters for the fast decay dynamics are shown here. Amplitudes of the first three decay components (Table S1 of the Supporting Information) are renormalized to 100% after subtraction of that of the 11.3 ns component (τ_4). Uncertainties in parameters are typically ~5%, estimated from one to three repeat measurements and also previously published results (*19*, *20*, *22*, *23*). [b]X is 7-deazaadenine.

multiple parallel quenching pathways due to coexisting different modes of base stacking interactions involving the ligand for which the crystal structures alone cannot account. Furthermore, these different modes of interactions apparently do not convert on a time scale faster than the picosecond time scale of fluorescence quenching dynamics.

Origins of the Quenching Dynamics. The three ultrafast decay components and their relative amplitudes (Table 1) represent a distribution of at least three subpopulations of different conformations with regard to the bound ligand that undergoes charge transfer with very different rates. The decay time scale of ~1 ps (τ_1) is faster than what one normally observes for 2AP quenching dynamics in nucleic acid structures (*27*, *36*) unless a

7-deazaguanine base is specifically incorporated and is well-stacked with 2AP (*19*, *20*). The presence of this component suggests that there is a very efficient charge transfer pathway for the 2AP ligand in a major subpopulation (51−61% population) resulting from a specific structural context. We suspect that this ~1 ps major decay component represents the ligand bound in the binding pocket exactly as in the structures observed by crystallography (*12*−*14*), where the ligand is held in place inside the pocket by multiple hydrogen bonds around the periphery of the entire ligand base (Figure 1). Note that although the ligand is not directly well stacked by any of the RNA bases in the binding pocket in these crystal structures (*12*−*14*), there are some degrees of simultaneous edge-to-edge overlap with multiple bases forming the ceiling and floor of the "hydrogen bonding cage" (Figure 1B). We can speculate that the ~1 ps ultrafast decay dynamics are not due to stacking of a single quencher base on the 2AP ligand, but it is possible that the entire hydrogen bonding cage structure with multiple edge-to-edge base overlaps with the ligand collectively provides an electronic environment that leads to excited states with high charge transfer character.

We recently demonstrated that incorporation of 7-deazaguanine can be very effective in analyzing possible role of guanine bases in quenching 2AP fluorescence to provide unambiguous site-specific information regarding the nature of direct stacking interactions in RNA motifs and can thus facilitate assignments of specific interactions (*19*, *20*, *22*). Charge transfer between 2AP and well-stacked adenine bases can occur on the 80−300 ps time scale, depending on the structural contexts (*27*, *36*). Generally, when a component on this time scale is observed and a particular adenine base is suspected of being the source of quenching through base stacking with the 2AP probe, the adenine base can be replaced with 7-deazaadenine (X) (Figure S3 of the Supporting Information) if such N7 to CH modification does not perturb the structure (e.g., hydrogen bonding or metal ion binding interaction involving N7 of purine). The base of X quenches 2AP on the time scale of a few picoseconds, faster than the natural adenine base (*23*), therefore converting the component on hundreds of picoseconds observed for the original RNA to a few picoseconds if the adenine in question is indeed involved in direct stacking with 2AP. By comparing the two decay profiles, one can determine such base stacking interaction with residue-specific precision. To identify the origin of the τ_3 components on the time scale of hundreds of picoseconds, we replaced three adenine bases, A21, A52, and A73, of each of the three riboswitches (Figure 1B) in the binding pocket individually with X. Replacements of such modified bases at these positions should not alter the native interactions involving these bases based on the crystal structures (*12*, *13*), and this was also confirmed by ITC measurements (Figure S5 and Table S2 of the Supporting Information). The ITC-determined binding affinity for *pbuE* WT RNA (3.8 μM) in 2 mM Mg^{2+} at 30 °C is similar to that measured by steady state fluorescence (1.4 μM) under the same conditions (*34*), and the affinity for *xpt-pbuX*-GR (C74U)-WT is higher at 10 mM Mg^{2+} (0.6 μM) than at 2 mM Mg^{2+} (1.6 μM), the former also similar to that reported previously (0.3−0.5 μM) (*14*, *15*). The X-mutated RNAs all have similar low micromolar affinities for the 2AP ligand compared to those for the WT RNAs (Table S2 of the Supporting Information), suggesting that the X substitutions at these positions do not disrupt the structures and interactions.

Figure 3 shows that via replacement of either A21 or A52 individually with X in all three RNAs, the amplitudes of the τ_3 components in all three RNA complexes are partially reduced and instead decays that (happen to) overlap with that of τ_2 in time scale emerge with higher amplitudes. Replacing A73, however, did not produce such significant changes in any of these RNAs compared to WT. The changes in the decay dynamics for A21X

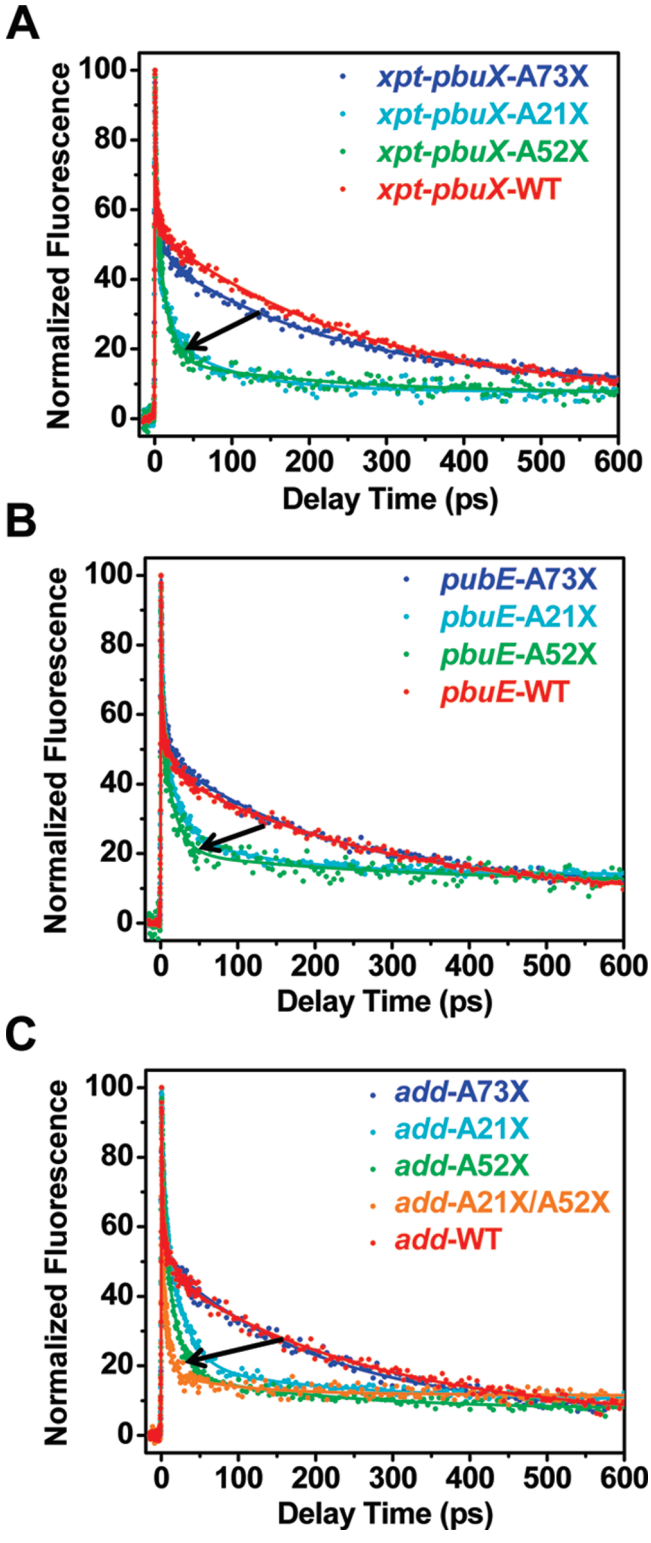

FIGURE 3: Comparison of decay profiles between WT constructs (red) and constructs with 7-deazaadenine (X) substituted at A21 (cyan), A52 (green), A73 (blue), or both A21 and A52 (orange) for (A) the *xpt-pbuX*-GR (C74U) riboswitch, (B) the *pbuE* A-riboswitch, and (C) the *add* A-riboswitch. Arrows indicate changes in time scale from slow in WT to fast in the A21X, A52X, and A21X/A52X mutants.

Table 2: Population Distributions of the 2AP Ligand Stacked with A21 and/or A52

	A21/ligand[a]	ligand/A52[b]	A21/ligand/A52[c]	total[d]
xpt-pbuX-GR (C74U)	8%	15%	11%	34%
pbuE-AR	8%	13%	7%	28%
add-AR	11%	10%	17%	38%

[a]Represents the subpopulation that the 2AP ligand stacks with A21 only; percentage is the same as amplitude A_3 of τ_3 for riboswitch mutant A52X (Table 1). [b]Represents the subpopulation that the 2AP ligand stacks with A52 only; percentage is the same as amplitude A_3 of τ_3 for riboswitch mutant A21X (Table 1). [c]Represents the subpopulation that the 2AP ligand stacks between A21 and A52, calculated as the difference between A_3 of the wild type and the sum of the A_3 amplitudes for the A21X and A52X mutants. [d]Correspond to A_3 amplitudes for WT.

and A52X mutants suggest that both A21 and A52, but not A73, are involved in separate well-defined structures that quench 2AP on a time scale of hundreds of picoseconds in all three RNAs. There are three possible populations that can contribute to τ_3 for the WT, i.e., 2AP stacking with A21 only, with A52 only, and with both A21 and A52. The remaining amplitudes of τ_3 for the A21X and A52X mutants represent the subpopulations in which the 2AP ligand is not stacked with A21 and A52, respectively. For example, for *xpt-pbuX*-GR (C74U), an amplitude of 34% of τ_3 for the WT is reduced to 15 and 8% in the A21X and A52X mutants, respectively. Simple calculations using these amplitude values show that of the 34% population, 8% (amplitude A_3 for the A52X mutant) is stacked with A21 only (ligand/A21), 15% (amplitude A_3 for the A21X mutant) is stacked with A52 only (A52/ligand), and 11% (difference in amplitude A_3 between WT and the sum of A21X and A52X) is stacked with both (sandwiched between A21 and A52, A52/ligand/A21). Similar calculations can be performed for the two adenine-sensing riboswitches (Table 2). Overall, there seem to be three substates, all characterized by τ_3, that are approximately similarly populated. These assignments predict that in a mutant where both A21 and A52 are replaced with X, the amplitude of τ_3 would be completely removed. Figure 3C shows the decay profile for such a mutant of the *add* riboswitch (*add*-A21X/A52X), where there is little amplitude of τ_3 (4%), consistent with the prediction that τ_3 dynamics are mostly due to interactions of the ligand with A21 and A52. These conformations of the ligand identified here are different from the crystal structures (Figure 1) which are most likely characterized by τ_1. Note that in the crystal structures, the two adenines (A21 and A52) are on the opposite edges of the ligand but not far from it (Figure 1B), so the ligand will have to undergo some conformational motion to sample these alternative conformations with well-defined base stacking interactions. Presumably, the binding pocket has to distort to some extent to accommodate the ligand motion.

The quenching time scale of the τ_2 component (5.5−11 ps) of small amplitudes (11%) for the WT RNAs, which represents a small subpopulation, is consistent with quenching of 2AP by uracil bases, possibly U22 and U75 (~5% subpopulation each on average), which happen to base pair with A52 and A21, respectively (Figure 1B). No specific base analogue that allows us to directly probe the role of these uracil bases as described above for adenines is available. However, we have tested this on a designed small model RNA construct with a 2AP-U pair (to mimic the 2AP-U74 pair) between two U-A pairs such that 2AP is inserted between the two U residues. The primary decay dynamics is a 10 ps component (Figure S4 of the Supporting

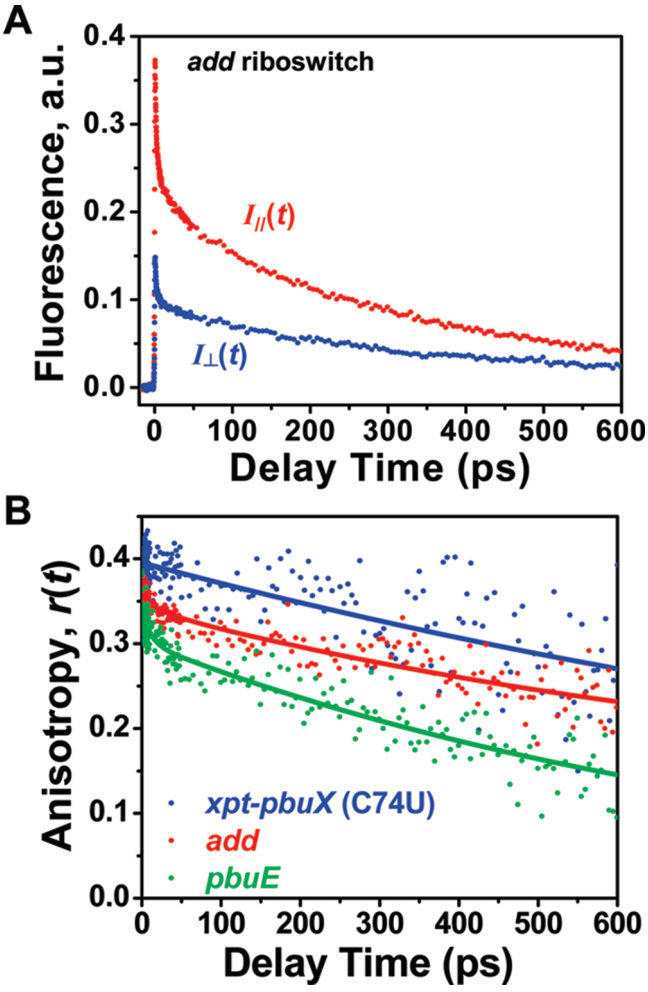

FIGURE 4: Ultrafast time-resolved fluorescence anisotropy decay of the 2AP ligand bound to riboswitches. (A) Fluorescence decays for 2AP bound to the *add* riboswitch with polarization parallel ($I_{//}$, red) or perpendicular ($I_{\perp}$, blue) to that of the excitation pulse. (B) Anisotropy decays of the 2AP ligand, $r(t)$, bound to *xpt-pbuX* (C74U) (blue, τ = 1.6 ns), *add* (red, τ = 1.0 ns), and *pbuE* (green, τ = 1.0 ns) riboswitches. Solid lines are the best fits. Uncertainties in parameters are 10−20%.

Information). Possibly, the 2AP ligand, while stacked between the two A21-U75 and A52-U22 base pairs of the binding pocket, can slide back and forth from stacking with the adenines to stacking with the uracils but apparently prefers the larger adenine bases, as the τ_3 values have larger amplitudes than the τ_2 values.

Dynamic Motions of the Ligand inside the Binding Pocket Probed by Ultrafast Time-Resolved Anisotropy. To probe the mobility of the ligand inside the binding pocket, we have collected femtosecond time-resolved fluorescence anisotropy decays of 2AP bound to the three WT riboswitches. If the ligand is tightly bound to the RNA without any internal motion, the anisotropy decay is expected to occur only on the time scale of the global tumbling rotation of the entire domain. For a complex of this size (~23 kDa), the expected rotational correlation time is ~10 ns (*24*). Local or internal motions, however, can promote the anisotropy decay to occur on faster time scales (*20*, *22*). Figure 4A shows the decays of fluorescence with polarization parallel or perpendicular to that of the excitation pulse for 2AP bound to *add* riboswitch RNA, and Figure 4B shows the constructed femtosecond time-resolved anisotropy decays of 2AP bound to the three WT riboswitches. Besides an ~12−20 ps component of

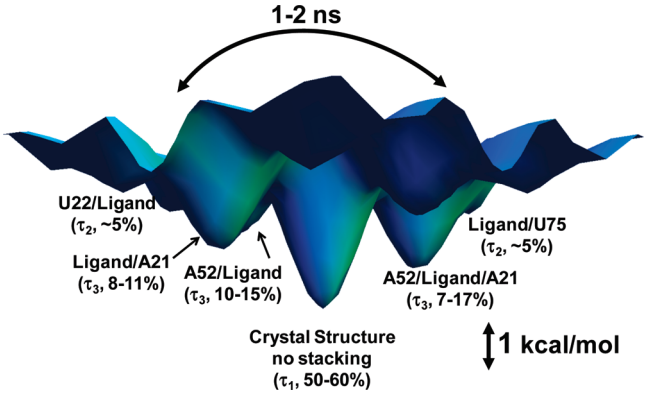

FIGURE 5: Models of the energy landscape for the 2AP ligand bound to all three of the purine-sensing riboswitch RNAs. The crystal structures regarding the ligand conformation represent the global minimum (no stacking, characterized by a τ_1 of ~1 ps, 50−60% population). The local minimum includes ligand stacking with A21 only (ligand/A21, 8−11%), stacking with A52 only (A52/ligand, 10−15%), or stacking with both A21 and A52 (A52/ligand/A21, 7−17%); all three are characterized by a τ_3 of ~249−283 ps with a total population of 28−38%. Minor populations of ligand stacking with either U22 or U75 (U22/ligand or U75/ligand, ~5% each) are characterized by a τ_2 of ~5.5−11 ps. The scale for $\Delta\Delta G^\circ$ and possible motions of conformational interconversion on the 1−2 ns time scale are indicated.

small amplitude that presumably represents the contribution from the residual free 2AP in solution for the two adenine-sensing RNAs and an ~10 ns component for the *add* RNA as the offset of its profile that represents the rotation of the entire domain, apparent anisotropy decays of 1.0, 1.0, and 1.6 ns [after deconvolution from the 10 ns domain rotation (*24*)] of significant amplitude are observed for the 2AP ligand bound to *add*, *pbuE*, and *xpt-pbuX* riboswitches, respectively. These anisotropy decay components represent the internal motion correlation times of the bound ligand, clearly indicating that the 2AP ligand undergoes a major dynamic motion inside the pocket on a time scale of 1−2 ns. Internal motion on picosecond to nanosecond time scales has previously been observed for 2AP covalently incorporated into regular double-stranded states (*20*, *22*). Therefore, the 1−2 ns internal dynamics observed here are probably slaves to the intrinsic motion of the binding pocket.

Note that this nanosecond time scale of base motion is different from all the observed ultrafast quenching dynamics on picosecond time scales measured under the magic angle condition (Figure 2 and Table 1). Therefore, the charge transfer chemical processes that caused the fluorescence decay on ultrafast time scales and the actual conformational dynamics of the ligand are well separated in the time domain. This suggests that the picosecond quenching dynamics discussed above are indeed due to direct static quenching between stacked bases on the ground state that is heterogeneous, not gated by rate-limiting conformational dynamics events. The observed nanosecond internal conformational dynamics of the 2AP ligand suggest that the kinetic barrier for some conformational transition is as low as a few kilocalories per mole. Therefore, magic angle and anisotropy experiments provide unique structural, thermodynamic, and kinetic information.

DISCUSSION

Multiple Conformations and Multiple Interaction Modes. Because ligand binding by riboswitches is a crucial step in riboregulation, as such an event triggers the switch mechanism, it is essential to understand the physical and chemical nature of the ligand recognition by riboswitches. Our femtosecond time-resolved spectroscopic probing suggested that for purine ligand recognition by the riboswitches, hydrogen bonding is not the only mode of interaction. There is a dynamic balance between hydrogen bonding and direct base stacking interactions that produces ligand binding affinity and specificity. Figure 5 presents a model for the conformational heterogeneity of the ligand in the bound state for the purine-sensing riboswitches. We were able to interpret the observed quenching dynamics in terms of specific conformations regarding the ligand. The population data (Tables 1 and 2) can be directly used in partition function analysis to calculate the free energy difference between any two distinct substates (*i* and *j*) at a given temperature *T* [$\Delta\Delta G^\circ_{i,j} = -RT \ln(A_i/A_j)$].

The bound ligand samples a few families of conformations. The available crystal structures most likely represent one of the major conformations which is the global minimum with the highest population (~50−60%), where the ligand is located between the two A21-U75 and A52-U22 base pairs but without significant direct base−base stacking except some overlap with the edge of the bases (Figure 2B). We can hypothesize that the minimal but multiple edge-to-edge base overlaps provide an electronic environment that promotes ultrafast quenching dynamics on the ~1 ps time scale (τ_1). It would be experimentally difficult to synthetically construct a small model system that precisely mimics the structure of the binding pocket with 2AP bound inside and use ultrafast time-resolved spectroscopy to determine whether there are ~1 ps decay dynamics. Such a hypothesis can potentially be tested by time-dependent density function theory (TDDFT) calculation, where the hydrogen bonding cage structure can be modeled as a supermolecule (*39*) to identify potential excited states that can act as an efficient radiation-less sink for the excited state of 2AP (*39*, *40*) in the context of the binding pocket structure of riboswitches. In a second major family of populations (total of 28−38%), the 2AP ligand stacks on A21 only (8−11%), A52 only (10−15%), or both (7−17%). These three subpopulations collectively provide an ~249−283 ps (τ_3) charge transfer pathway due to quenching by adenines (not individually resolved for each complex due to similar time scales). The free energy difference ($\Delta\Delta G^\circ_{22\ ^\circ C}$) between the two major families of conformations (5:1 to 6:1 A_1:A_2 ratios) is ~1 kcal/mol. These two major families of conformations are in dynamic exchange with a minor population (11%) characterized by the 5.5−11 ps component (τ_2) due to stacking of 2AP with U22 or U75 (on average ~5% each, $\Delta\Delta G^\circ_{22\ ^\circ C}$ ~ 1.4−1.5 kcal/mol relative to the global minimum). A recent calculation was conducted to deconstruct the ligand binding energy into different interaction modes (*41*) that also suggested significant contributions from base stacking interaction involving the bases forming the pocket. The largely non-specific nature of base stacking interactions and its dynamic nature significantly contribute to the ruggedness of the RNA conformational landscape (Figure 5). Apparently, the model presented in Figure 5 concerns only the bound ligand and represents the intricate details of the portion of the landscape of the entire ligand binding conformational trajectory presented by others which included the free energy landscape of free RNA states and initial ligand docking (*42*−*45*). In addition, each of these different structures inferred from the ultrafast dynamics probing should still be considered as potentially a family of

related structures, because the current data set alone reveals only local information on the ligand itself, and structures of the aptamer domain that may feature global and local differences elsewhere but collectively happen to produce the same local stacking environment for the 2AP ligand would behave the same way in this probing.

The A21-U75 pair is a highly conserved base pair but appears to have a limited direct impact on ligand binding (*35*, *46*). The crystal structure of 2,6-diaminopurine−RNA complexes with different base pairs at this position appears to have essentially identical folds (*46*). However, this base pair may affect the intrinsic flexibility of base Y74 depending on the number of hydrogen bonding interactions and, therefore, influence the specificity of ligand recognition (*16*). The U22-A52 pair can be changed to a C22-G52 pair without a significant reduction in ligand binding affinity (*46*). This mutation was in fact observed in the 2′-dG riboswitch (*47*). Changing the U22-A52 pair to either a AU or a GC pair, however, leads to significant loss of binding due to possible formation of an alternative R22-Y74 pair in the free state of RNA, thereby impairing ligand binding (*46*). Our ultrafast dynamics data suggest that in addition to their roles in influencing the flexibility and availability of Y74 in the ligand-free states, bases of these two pairs directly stack with the ligand with significant overlap in some subpopulations (total amplitudes of A_2 and A_3, 39−49%) of the complexed state. Presumably, the switch of positions between the purine base and the pyrimidine base of the U22-A52 pair would cause a change in the stacking energies as the purine ligand prefers a larger purine base at position 52, partially explaining the preference for Y22-R52 pairs over R22-Y52 pairs (*46*).

Dynamic Motions of the Ligand on the Nanosecond Time Scale. On the basis of the crystal structures of both adenine- and guanine-sensing riboswitches, the purine ligand is almost completely buried inside the RNAs and is held in place through multiple hydrogen bonding interactions (*12*−*14*). A smaller pyrimidine analogue ligand does not appear to induce any adjustment (collapse) of the pocket of the *xpt-pbuX*-GR (C74U) riboswitch (*15*). These findings suggested that the pocket is rather rigid, at least in the bound state. Recently, however, small alterations in the shape of the binding pocket (e.g., minor groove wobbling of the specificity base Y74) have been observed to accommodate a number of ligand analogues with additional or different displays of functional groups at position 2 or 6 (*16*), indicating that the pocket can also adapt to changes in the ligand shape. A variant of the guanine riboswitch (I-A) was recently discovered that senses 2′-dG (*47*), and the structure of its aptamer domain is very similar to those of A- and G-riboswitches. The switch of specificity appeared to be due to a small number of nucleotide changes, e.g., U51C, in the highly conserved core region, leading to small changes in the position of C51 in the binding pocket compared to that of U51 in the G-riboswitch to accommodate the additional 2′-deoxyribose moiety (*48*). Recently, orthogonal selectivity to accommodate ligands such as ammeline and azacytosin with respect to the parental *add* riboswtich yielded mutations of U47 to C47 and U51 to C51 (*49*), where C51 makes a lateral movement away from C47 that is similar to the movement observed in the 2′-dG riboswitch. Such altered specificity by a small number of base changes has been observed for small RNA aptamers. For example, an aptamer that recognizes citrulline can be altered to recognize arginine with a change of three of 44 nucleotides (*50*) without significant changes in the folded structure (*51*). Similarly, a highly specific theophylline-binding aptamer (*52*, *53*) can be changed to recognize 3-methylxanthine with a single base mutation (*54*).

Although the observed changes in the ligand binding pocket of various riboswitch complexes are induced by either the presence of an altered ligand shape (*16*, *49*) or an additional ligand moiety (*48*), we can hypothesize that flexibility is intrinsic to these RNAs and such structural alterations of the binding pocket can also be sampled by excursion of the WT complexes with the bound cognate ligand. In particular, bases 47−49 and 51 may sample a number of different but closely related conformations, some of which can be stabilized by specific ligand interactions, including stacking. The presence of multiple picosecond decay components we observed for the bound 2AP ligand suggests that there are indeed coexisting alternative stacking structures involving the ligand. This implies that the ligand may undergo a certain degree of motion inside the pocket with concurrent motion of the bases forming the pocket on a distinct time scale that allows it to sample these different states. The observed charge transfer rates measured under the magic angle condition discussed above reflect only the electronic interactions between the probe and quencher bases that help identify the presence of alternative conformations and define the nature of such conformations; they do not directly represent the RNA base motions per se.

The anisotropy decay measurements for the WT riboswitches revealed that the bound ligand undergoes motions on the nanosecond time scale inside the binding pocket. This suggests that some types of conformational transitions involving the ligand can occur on a 1−2 ns time scale indicating a low activation energy barrier. Such motions of the ligand are most likely coupled to base motions of the RNAs, at least the bases forming the binding pocket, but possibly even the entire RNA aptamer domain globally (see below). It is tempting to speculate that this 1−2 ns conformational transition may be the sliding of 2AP between stacking with the two adenines and stacking with the two uracils, and the ligand position in the crystal structure is on the pathway of such base sliding. Molecular dynamics simulation of the G-riboswitch (*55*) and A-riboswitch (*56*, *57*) in the ligand-bound state indicated that there are nanosecond fluctuations of the ligand in the binding pocket leading to at least two populations with altered stacking interactions between the ligand and the base triples forming the ceiling and floor of the pocket, supporting our observations of multiple base stacking interaction modes. In particular, nanosecond hydrogen bonding dynamics involving the adenine ligand leads to stronger stacking with A21 when A21 undergoes partial base pair opening with U75 (*57*).

Comparison to Previous Nanosecond Time-Resolved Fluorescence Spectroscopy. In the nanosecond time-resolved probing of the 2AP ligand bound to the *pbuE* A-riboswitch (*25*) and the *xpt-pbuX* G-riboswitch (*26*), a fluorescence lifetime of < 300 ps with an ~60% amplitude was invoked to account for the unresolved static quenching regime of the nanosecond decay profile and was assigned to the folded conformation observed by crystallography. Structural heterogeneity due to global transient opening of the L2 loop−L3 loop interactions was proposed to account for the multiple lifetimes of the bound 2AP ligand on the nanosecond time scale, and conformations with such opening of tertiary interactions can lead to a significant loss of ligand binding affinity and higher sensitivity to Mg^{2+} (*26*, *58*). The nanosecond time-resolved studies and the femtosecond time-

resolved study are complementary and have partial overlap around the subnanosecond time regime (see a simulation of combined data from both studies in Figure S5 of the Supporting Information). The ultrafast decay dynamics have now been fully resolved here. The < 300 ps component and at least most of the subnanosecond (~0.5 ns) component in the nanosecond studies correspond to τ_1 and τ_2 with a large total amplitude mixed with the τ_3 component in our femtosecond time-resolved probing. Our observations indicate that even in the subpopulation of the fully folded or closed state, there are still significant local heterogeneous conformational substates of the ligand in the binding pocket giving rise to the multiphasic decay profiles in the ultrafast time regime. The experimentally observed conformational heterogeneity is consistent with the MD simulation in which local motions of the ligand lead to alternative conformations inside the pocket (*55*, *57*). However, on the basis of our observations, few decay components beyond 1 ns are observed in the femtosecond time-resolved decay, and the decay profiles feature mostly quenching dynamics within 1 ns. It is possible that the nanosecond time scale base motions of the ligand observed from anisotropy decay measurements act to gate the charge transfer reaction (*59*) and give rise to an apparent charge transfer rate on the ~2 ns time scale observed in the earlier studies (*25*, *26*). It should be noted that the P1 stem for the *pbuE* A-riboswitch used in the nanosecond time-resolved studies is shorter than that use in the work reported here, which may render the RNA more dynamic globally and potentially contribute to the presence of the nanosecond decay component hypothesized to represent the open state in that study. The extended or stabilized P1 stem has previously been used extensively in NMR (*44*, *60*−*63*) and fluorescence (*34*, *37*) studies. The robustness of the dynamics decay profiles in the picosecond to nanosecond time regime among all three riboswitches observed in the femtosecond study (Figure 2) and the similar decay profiles between the *pubE* A-riboswitch with a shorter P1 stem and the *xpt-pbuX* G-riboswich observed in the nanosecond time regime (*26*), however, all indicate that it is the local structure of the binding pocket, not the overall stability of the P1 stem, that dominates the dynamic behaviors of the ligand.

These time-resolved studies alone, however, cannot definitively reveal whether or how these local dynamics are coupled to any global conformational dynamics of the riboswitch aptamer domains, particularly because these large scale conformational dynamics would occur on a time scale much slower than the lifetime of 2AP. Single-molecule FRET approaches have provided unique insights into this question. It has been shown that the adenine and guanine riboswitches have a single conformation when the ligand is bound in the presence of ≥2 mM Mg^{2+} (*37*, *64*), suggesting that the multiple conformations that we have observed are more likely due to local heterogeneity only, not global conformational fluctuation. In other words, the presence of these different conformations reflects the elasticity, not the plasticity, of the purine ligand recognition by these riboswitches.

Rugged Energy Landscape of the Ligand-Free State. The binding pocket entirely engulfs the ligand (Figure 1A,B), suggesting that ligand recognition must be coupled to a reorganization event at least locally (*12*). Perhaps one of the strands in the junction region is dynamic to open the gateway for the ligand to gain access (*58*, *65*), although there also must be some preorganization to reduce the total entropic penalty (*14*, *46*). No crystal structures of these riboswitches free of ligands are currently available perhaps because of their highly dynamic and heterogeneous nature, but studies using fluorescence (*34*, *35*, *65*), ITC (*14*, *58*), NMR (*44*, *61*, *62*), single-molecule FRET (*37*), single-molecule force spectroscopy (*42*, *45*), and simulations (*55*, *56*) all suggested that the free RNAs exist as multiple interconverting conformers, one of which may be competent for ligand binding. All of these conformational transitions are consequences of dynamics that occur on different time scales, including fast and slow events. However, the exact nature of the structural ensemble and dynamics in the ligand-free state and the conformational rearrangements and changes in the dynamics caused by ligand binding are currently some of the most significant remaining unresolved issues (*7*, *66*) and await investigation by appropriate approaches. However, the relatively low *n* values (number of binding sites) from our ITC data (Table S2 of the Supporting Information) seem to suggest that less than half of the free RNA can convert to a complex in the presence of the ligand within the time scale of the ITC experiments, consistent with the necessity of using an RNA:2AP ratio of at least 4:1 to saturate the ligand for fluorescence dynamics probing even at concentrations well above K_d values. An *n* value of less than unity from ITC measurements has been reported in the literature (*15*, *46*), and such information is typically not revealed in steady state fluorescence titration. Although purine ligands form 1:1 complexes with purine-sensing riboswitches when they are bound, these observations suggested that there is a barrier in the free RNA state. Such a phenomenon of conformational ruggedness where distinct folded states do not interconvert on an observable experimental time scale has been observed in a few other RNA structures (*67*−*69*). It is still not clear, however, whether this phenomenon is dominated by configurational or conformational origin, despite biochemical and biophysical analyses that included the use of single-molecule techniques, and this deserves further investigation. Ultrafast time-resolved spectroscopy, with its ability to resolve complex population distributions of a conformational ensemble (*21*), can complement single-molecule approaches (*68*, *69*) and contribute to our understanding of RNA dynamics and their role in molecular recognition.

SUPPORTING INFORMATION AVAILABLE

Steady state emission spectra, chemical structures of purine bases, table of full decay parameters, residual plots and simulation of full decay dynamics for *pbuE* RNA, decay dynamics of the model RNA system, and figures and table of ITC data. This material is available free of charge via the Internet at http://pubs.acs.org.

REFERENCES

1. Crothers, D. M. (2001) RNA Conformational Dynamics. In RNA (Soll, D., Nishimura, S., and Moore, P. B., Eds.) pp 61−70, Elsevier Science Ltd., Oxford, U.K.
2. Williamson, J. R. (2000) Induced fit in RNA-protein recognition. *Nat. Struct. Biol. 7*, 834–837.
3. Leulliot, N., and Varani, G. (2001) Current topics in RNA-protein recognition: Control of specificity and biological function through induced fit and conformational capture. *Biochemistry 40*, 7947–7956.
4. Al-Hashimi, H. M., and Walter, N. G. (2008) RNA Dynamics: It is about time. *Curr. Opin. Struct. Biol. 18*, 321–329.
5. Winkler, W. C., and Breaker, R. R. (2005) Regulation of bacterial gene expression by riboswitches. *Annu. Rev. Microbiol. 59*, 487–517.
6. Barrick, J. E., and Breaker, R. R. (2007) The distributions, mechanisms, and structures of metabolite-binding riboswitches. *Genome Biol. 8*, R239.

7. Montange, R. K., and Batey, R. T. (2008) Riboswitches: Emerging themes in RNA structure and function. *Annu. Rev. Biophys. 37*, 117–133.
8. Blount, K. F., and Breaker, R. R. (2006) Riboswitches as antibacterial drug targets. *Nat. Biotechnol. 24*, 1558–1564.
9. Kim, J. N., and Breaker, R. R. (2008) Purine sensing by riboswitches. *Biol. Cell 100*, 1–11.
10. Mandal, M., Boese, B., Barrick, J. E., Winkler, W. C., and Breaker, R. R. (2003) Riboswitches control fundamental biochemical pathways in *Bacillus subtilis* and other bacteria. *Cell 113*, 577–586.
11. Mandal, M., and Breaker, R. R. (2004) Adenine riboswitches and gene activation by disruption of a transcription terminator. *Nat. Struct. Mol. Biol. 11*, 29–35.
12. Batey, R. T., Gilbert, S. D., and Montange, R. K. (2004) Structure of a natural guanine-responsive riboswitch complexed with the metabolite hypoxanthine. *Nature 432*, 411–415.
13. Serganov, A., Yuan, Y.-R., Pikovskaya, O., Polonskaia, A., Malinina, L., Phan, A. T., Hobartner, C., Micura, R., Breaker, R. R., and Patel, D. J. (2004) Structural Basis for Discriminative Regulation of Gene Expression by Adenine- and Guanine-Sensing mRNAs. *Chem. Biol. 11*, 1729–1741.
14. Gilbert, S. D., Stoddard, C. D., Wise, S. J., and Batey, R. T. (2006) Thermodynamic and kinetic characterization of ligand binding to the purine riboswitch aptamer domain. *J. Mol. Biol. 359*, 754–768.
15. Gilbert, S. D., Mediatore, S. J., and Batey, R. T. (2006) Modified Pyrimidines Specifically Bind the Purine Riboswitch. *J. Am. Chem. Soc. 128*, 14214–14215.
16. Gilbert, S. D., Reyes, F. E., Edwards, A. L., and Batey, R. T. (2009) Adaptive ligand binding by the purine riboswitch in the recognition of guanine and adenine analogs. *Structure 17*, 857–868.
17. Xia, T., Becker, H. C., Wan, C., Frankel, A., Roberts, R. W., and Zewail, A. H. (2003) The RNA-protein complex: Direct probing of the interfacial recognition dynamics and its correlation with biological functions. *Proc. Natl. Acad. Sci. U.S.A. 100*, 8119–8123.
18. Xia, T., Wan, C. Z., Roberts, R. W., and Zewail, A. H. (2005) RNA-protein recognition: Single-residue ultrafast dynamical control of structural specificity and function. *Proc. Natl. Acad. Sci. U.S.A. 102*, 13013–13018.
19. Zhao, L., and Xia, T. (2007) Direct Revelation of Multiple Conformations in RNA by Femtosecond Dynamics. *J. Am. Chem. Soc. 129*, 4118–4119.
20. Liu, J. D., Zhao, L., and Xia, T. (2008) The Dynamic Structural Basis of Differential Enhancement of Conformational Stability by 5′- and 3′-Dangling Ends in RNA. *Biochemistry 47*, 5962–5975.
21. Xia, T. (2008) Taking femtosecond snapshots of RNA conformational dynamics and complexity. *Curr. Opin. Chem. Biol. 12*, 604–611.
22. Kadakkuzha, B. M., Zhao, L., and Xia, T. (2009) Conformational Distribution and Ultrafast Base Dynamics of Leadzyme. *Biochemistry 48*, 3807–3809.
23. Zhao, L., and Xia, T. (2009) Probing RNA Conformational Dynamics and Heterogeneity Using Femtosecond Time-resolved Fluorescence Spectroscopy. *Methods 49*, 128–135.
24. Lakowicz, J. R. (1999) Principles of Fluorescence Spectroscopy, 2nd ed., Kluwer Academic/Plenum Plublishers, New York.
25. Eskandari, S., Prychyna, O., Leung, J., Avdic, D., and O'Neill, M. A. (2007) Ligand-Directed Dynamics of Adenine Riboswitch Conformers. *J. Am. Chem. Soc. 129*, 11308–11309.
26. Prychyna, O., Dahabieh, M. S., Chao, J., and O'Neill, M. A. (2009) Sequence-Dependent Folding and Unfolding of Ligand-Bound Purine Riboswitches. *Biopolymers 91*, 953–965.
27. Fiebig, T., Wan, C., and Zewail, A. H. (2002) Femtosecond Charge Transfer Dynamics of a Modified DNA Base: 2-Aminopurine in Complexes with Nucleotides. *ChemPhysChem 3*, 781–788.
28. Wan, C., Fiebig, T., Schiemann, O., Barton, J. K., and Zewail, A. H. (2000) Femtosecond direct observation of charge transfer between bases in DNA. *Proc. Natl. Acad. Sci. U.S.A. 97*, 14052–14055.
29. Pal, S. K., Peon, J., and Zewail, A. H. (2002) Ultrafast decay and hydration dynamics of DNA bases and mimics. *Chem. Phys. Lett. 363*, 57–63.
30. Pal, S. K., Zhao, L., Xia, T., and Zewail, A. H. (2003) Site- and sequence-selective ultrafast hydration of DNA. *Proc. Natl. Acad. Sci. U.S.A. 100*, 13746–13751.
31. Andreatta, D., Lustres, J. L. P., Kovalenko, S. A., Ernsting, N. P., Murphy, C. J., Coleman, R. S., and Berg, M. A. (2005) Power-law solvation dynamics in DNA over six decades in time. *J. Am. Chem. Soc. 127*, 7270–7271.
32. Holmen, A., Norden, B., and Albinsson, B. (1997) Electronic Transition Moments of 2-Aminopurine. *J. Am. Chem. Soc. 119*, 3114–3121.
33. Gilbert, S. D., and Batey, R. T. (2009) Monitoring RNA-ligand interactions using isothermal titration calorimetry. *Methods Mol. Biol. 540*, 97–114.
34. Wickiser, J. K., Cheah, M. T., Breaker, R. R., and Crothers, D. M. (2005) The kinetics of ligand binding by an adenine-sensing riboswitch. *Biochemistry 44*, 13404–13414.
35. Lemay, J. F., and Lafontaine, D. A. (2007) Core requirements of the adenine riboswitch aptamer for ligand binding. *RNA 13*, 339–350.
36. Wan, C. Z., Xia, T. B., Becker, H. C., and Zewail, A. H. (2005) Ultrafast unequilibrated charge transfer: A new channel in the quenching of fluorescent biological probes. *Chem. Phys. Lett. 412*, 158–163.
37. Lemay, J. F., Penedo, J. C., Tremblay, R., Lilley, D. M. J., and Lafontaine, D. A. (2006) Folding of the adenine riboswitch. *Chem. Biol. 13*, 857–868.
38. Berg, M. A., Coleman, R. S., and Murphy, C. J. (2008) Nanoscale structure and dynamics of DNA. *Phys. Chem. Chem. Phys. 10*, 1229–1242.
39. Jean, J. M., and Hall, K. B. (2002) 2-Aminopurine electronic structure and fluorescence properties in DNA. *Biochemistry 41*, 13152–13161.
40. Jean, J. M., and Hall, K. B. (2001) 2-Aminopurine fluorescence quenching and lifetimes: Role of base stacking. *Proc. Natl. Acad. Sci. U.S.A. 98*, 37–41.
41. Sharma, P., Sharma, S., Chawla, M., and Mitra, A. (2009) Modeling the noncovalent interactions at the metabolite binding site in purine riboswitches. *J. Mol. Model. 15*, 633–649.
42. Greenleaf, W. J., Frieda, K. L., Foster, D. A. N., Woodside, M. T., and Block, S. M. (2008) Direct observation of hierarchical folding in single riboswitch aptamers. *Science 319*, 630–633.
43. Gilbert, S. D., and Batey, R. T. (2006) Riboswitches: Fold and function. *Chem. Biol. 13*, 805–807.
44. Buck, J., Furtig, B., Noeske, J., Wohnert, J., and Schwalbe, H. (2007) Time-Resolved NMR methods resolving ligand-induced RNA folding at atomic resolution. *Proc. Natl. Acad. Sci. U.S.A. 104*, 15699–15704.
45. Lin, J. C., and Thirumalai, D. (2008) Relative stability of helices determines the folding landscape of adenine riboswitch aptamers. *J. Am. Chem. Soc. 130*, 14080–14081.
46. Gilbert, S. D., Love, C. E., Edwards, A. L., and Batey, R. T. (2007) Mutational analysis of the purine riboswitch aptamer domain. *Biochemistry 46*, 13297–13309.
47. Kim, J. N., Roth, A., and Breaker, R. R. (2007) Guanine riboswitch variants from *Mesoplasma florum* selectively recognize 2′-deoxyguanosine. *Proc. Natl. Acad. Sci. U.S.A. 104*, 16092–16097.
48. Edwards, A. L., and Batey, R. T. (2009) A structural basis for the recognition of 2′-deoxyguanosine by the purine riboswitch. *J. Mol. Biol. 385*, 938–948.
49. Dixon, N., Duncan, J. N., Geerlings, T., Dunstan, M. S., McCarthy, J. E., Leys, D., and Micklefield, J. (2010) Reengineering orthogonally selective riboswitches. *Proc. Natl. Acad. Sci. U.S.A. 107*, 2830–2835.
50. Famulok, M. (1994) Molecular Recognition of Amino-Acids by RNA-Aptamers: An L-Citrulline Binding RNA Motif and Its Evolution into an L-Arginine Binder. *J. Am. Chem. Soc. 116*, 1698–1706.
51. Yang, Y. S., Kochoyan, M., Burgstaller, P., Westhof, E., and Famulok, M. (1996) Structural basis of ligand discrimination by two related RNA aptamers resolved by NMR spectroscopy. *Science 272*, 1343–1347.
52. Jenison, R. D., Gill, S. C., Pardi, A., and Polisky, B. (1994) High-Resolution Molecular Discrimination by RNA. *Science 263*, 1425–1429.
53. Zimmermann, G. R., Jenison, R. D., Wick, C. L., Simorre, J. P., and Pardi, A. (1997) Interlocking structural motifs mediate molecular discrimination by a theophylline-binding RNA. *Nat. Struct. Biol. 4*, 644–649.
54. Soukup, G. A., Emilsson, G. A. M., and Breaker, R. R. (2000) Altering molecular recognition of RNA aptamers by allosteric selection. *J. Mol. Biol. 298*, 623–632.
55. Villa, A., Wohnert, J., and Stock, G. (2009) Molecular dynamics simulation study of the binding of purine bases to the aptamer domain of the guanine sensing riboswitch. *Nucleic Acids Res. 37*, 4774–4786.
56. Sharma, M., Bulusu, G., and Mitra, A. (2009) MD simulations of ligand-bound and ligand-free aptamer: Molecular level insights into the binding and switching mechanism of the add A-riboswitch. *RNA 15*, 1673–1692.
57. Priyakumar, U. D., and Mackerell, A. D., Jr. (2010) Role of the Adenine Ligand on the Stabilization of the Secondary and Tertiary Interactions in the Adenine Riboswitch. *J. Mol. Biol. 396*, 1422–1438.

58. Stoddard, C. D., Gilbert, S. D., and Batey, R. T. (2008) Ligand-dependent folding of the three-way junction in the purine riboswitch. *RNA 14*, 675–684.
59. O'Neill, M. A., Becker, H. C., Wan, C., Barton, J. K., and Zewail, A. H. (2003) Ultrafast dynamics in DNA-mediated electron transfer: Base gating and the role of temperature. *Angew. Chem., Int. Ed. 42*, 5896–5900.
60. Noeske, J., Richter, C., Grundl, M. A., Nasiri, H. R., Schwalbe, H., and Wohnert, J. (2005) An intermolecular base triple as the basis of ligand specificity and affinity in the guanine- and adenine-sensing riboswitch RNAs. *Proc. Natl. Acad. Sci. U.S.A. 102*, 1372–1377.
61. Noeske, J., Buck, J., Furtig, B., Nasiri, H. R., Schwalbe, H., and Wohnert, J. (2007) Interplay of 'induced fit' and preorganization in the ligand induced folding of the aptamer domain of the guanine binding riboswitch. *Nucleic Acids Res. 35*, 572–583.
62. Noeske, J., Schwalbe, H., and Wohnert, J. (2007) Metal-ion binding and metal-ion induced folding of the adenine-sensing riboswitch aptamer domain. *Nucleic Acids Res. 35*, 5262–5273.
63. Ottink, O. M., Rampersad, S. M., Tessari, M., Zaman, G. J. R., Heus, H. A., and Wijmenga, S. S. (2007) Ligand-induced folding of the guanine-sensing riboswitch is controlled by a combined predetermined-induced fit mechanism. *RNA 13*, 2202–2212.
64. Brenner, M. D., Scanlan, M. S., Nahas, M. K., Ha, T., and Silverman, S. K. (2010) Multivector Fluorescence Analysis of the xpt Guanine Riboswitch Aptamer Domain and the Conformational Role of Guanine. *Biochemistry 49*, 1596–1605.
65. Rieder, R., Lang, K., Graber, D., and Micura, R. (2007) Ligand-induced folding of the adenosine deaminase A-riboswitch and implications on riboswitch translational control. *ChemBioChem 8*, 896–902.
66. Stoddard, C. D., and Batey, R. T. (2009) Beyond Crystallography: Investigating the Conformational Dynamics of the Purine-Riboswitch. In Non-Protein Coding RNAs (Walter, N. G., Woodson, S. A., and Batey, R. T., Eds.) pp 215−228, Springer-Verlag, Berlin.
67. Korennykh, A. V., Plantinga, M. J., Correll, C. C., and Piccirilli, J. A. (2007) Linkage between substrate recognition and catalysis during cleavage of sarcin/ricin loop RNA by restrictocin. *Biochemistry 46*, 12744–12756.
68. Ditzler, M. A., Rueda, D., Mo, J. J., Hakansson, K., and Walter, N. G. (2008) A rugged free energy landscape separates multiple functional RNA folds throughout denaturation. *Nucleic Acids Res. 36*, 7088–7099.
69. Solomatin, S. V., Greenfeld, M., Chu, S., and Herschlag, D. (2010) Multiple native states reveal persistent ruggedness of an RNA folding landscape. *Nature 463*, 681–684.